Inverse relationship between carrier mobility and bandgap in graphene

Cite as: J. Chem. Phys. **138**, 084701 (2013); https://doi.org/10.1063/1.4792142
Submitted: 28 October 2012 • Accepted: 28 January 2013 • Published Online: 22 February 2013

Jinying Wang, Ruiqi Zhao, Mingmei Yang, et al.

Inverse relationship between carrier mobility and bandgap in graphene

Jinying Wang,[1] Ruiqi Zhao,[1,2] Mingmei Yang,[1] Zhongfan Liu,[1,a)] and Zhirong Liu[1,a)]
[1]*College of Chemistry and Molecular Engineering, Beijing National Laboratory for Molecular Sciences (BNLMS), and Center for Nanochemistry, Peking University, Beijing 100871, China*
[2]*College of Physics and Chemistry, Henan Polytechnic University, Henan 454003, China*

(Received 28 October 2012; accepted 28 January 2013; published online 22 February 2013)

A frequently stated advantage of gapless graphene is its high carrier mobility. However, when a nonzero bandgap is opened, the mobility drops dramatically. The hardness to achieve high mobility and large on/off ratio simultaneously limits the development of graphene electronics. To explore the underlying mechanism, we investigated the intrinsic mobility of armchair graphene nanoribbons (AGNRs) under phonon scattering by combining first-principles calculations and a tight-binding analysis. A linear dependence of the effective mass on bandgap was demonstrated to be responsible for the inverse mobility-gap relationship. The deformation-potential constant was found to be determined by the strain dependence of the Fermi energy and the bandgap, resulting in two mobility branches, and is essential for the high mobility of AGNRs. In addition, we showed that the transport polarity of AGNRs can be switched by applying a uniaxial strain. © *2013 American Institute of Physics*. [http://dx.doi.org/10.1063/1.4792142]

I. INTRODUCTION

An extraordinary advantage of graphene lies in its ultrahigh carrier mobility at room temperature. In suspended graphene devices,[1–3] the mobility can reach as high as 2×10^5 cm^2 V^{-1} s^{-1} after the impacts of residual impurities are removed. This value is about two orders of magnitude larger than that in silicon. Even if substrates are used to support graphene, the measured mobility is still as high as $2 \sim 4 \times 10^4$ cm^2 V^{-1} s^{-1} on single-crystal hexagonal boron nitride (*h*-BN) substrate.[4] To facilitate graphene's applications in logic transistors, a bandgap needs to be opened to attain a large on/off ratio. Various methods have been applied to tailor the bandgap of graphene, e.g., by quantum confinement,[5,6] by chemical modification,[7–9] and by hybridization.[10,11] However, the carrier mobility of graphene reduced greatly as the bandgap increased. For example, sub-10 nm graphene nanoribbon field-effect transistors showed that the mobility dropped to less than 200 cm^2 V^{-1} s^{-1} with diminishing width when sufficient bandgap was opened.[12] Theoretical studies indicated that lateral confinement might suppress the intrinsic mobility of graphene nanoribbons (GNRs) to be much lower than the impressive value for two-dimensional (2D) graphene.[13,14] Such an inverse relationship between mobility and bandgap generally exists in various semiconductors,[15] which is an inevitable problem for graphene's electronic applications.

Various scattering processes affect the carrier mobility of graphene. Scattering from extrinsic sources such as charge impurities[16–18] can be eliminated or reduced significantly by improving sample preparation. Scatters such as phonons, however, cannot be removed at room temperature and thus limit the intrinsic mobility of graphene.[19] Much effort has been devoted to determining the intrinsic mobility of graphene and GNRs.[1–3,13,14,20–22] Phonon scattering was shown to dominate graphene's intrinsic mobility, and the in-plane and the out-of-plane (flexible) phonons have different temperature dependence.[21,22] For armchair graphene nanoribbons (AGNRs), it was revealed that the mobility of electrons and holes differed by two orders of magnitude and the transport polarity depended sensitively on the ribbon width.[20]

The electronic properties of graphene and GNRs are mainly determined by the π electrons, and can be well described with a simple theoretical framework.[23,24] It would be intriguing to adopt such a universal framework to investigate how the inverse mobility-gap relationship is produced in graphene-related systems, to elucidate various factors that influence the intrinsic mobility, and to explore possible means to regulate the mobility. In this work, we combined first-principles calculations with a tight-binding model analysis to address these questions. A quantitative/semiquantitative physical explanation is given for the mobility properties for both graphene and AGNRs, and strain is demonstrated to act as an effective means in switching the transport polarity of AGNRs.

II. METHOD AND MODEL

A. Formula of intrinsic mobility under phonon scattering

The influence of phonon scattering on the carrier mobility was described by the deformation potential theory.[25] For one-dimensional (1D) systems such as GNRs, an analytical expression for the mobility (μ) was derived:[26]

$$\mu = \frac{e\hbar^2 C}{(2\pi k_B T)^{1/2} |m^*|^{3/2} E_1^2}, \quad (1)$$

where T is the temperature with $T = 298$ K being adopted in our study and m^* is the effective mass of the charge

a)Authors to whom correspondence should be addressed. Electronic addresses: zfliu@pku.edu.cn and LiuZhiRong@pku.edu.cn.

carriers, defined as $m^* = \hbar^2(\partial^2 E(k)/\partial k^2)^{-1}$. C is the stretching modulus caused by the uniaxial-strain (ε), which can be calculated from $C = \frac{1}{a_0}\frac{\partial^2 E_{\text{total}}}{\partial \varepsilon^2}$ in which E_{total} is the total energy of a unit cell and a_0 is the equilibrium lattice constant. E_1 is the deformation-potential constant to denote the shift of the band-edge energy induced by ε, calculated using $E_1 = \frac{\partial E_{\text{edge}}}{\partial \varepsilon}$, where E_{edge} is the energy of the conduction band minimum (for electrons) or the valence band maximum (for holes). Equation (1) has been successfully applied to study the intrinsic mobility of GNRs[20] and graphyne nanoribbons.[27]

B. First-principles calculations

To calculate all these quantities, geometry optimization and electronic structure calculations for graphene and AGNRs with various ribbon widths (measured by the number N_A of dimer lines across the ribbon) were performed using density functional theory (DFT) implemented in Vienna *ab initio* simulation package.[28] The projector-augmented-wave pseudopotential[29] with the general gradient approximation of PW91 exchange correlation functional[30] was adopted, and the cutoff energy was 520 eV. The geometry was relaxed until all atomic forces were less than 0.01 eV/ Å, and at each self-consistent field iteration the convergence criterion for the total energy was 0.01 meV. We used large enough supercells in which the adjacent sheets were separated by at least 15 Å. All dangling bonds at the edge of AGNRs were saturated by hydrogen atoms.

C. Analysis with a tight-binding model

The effective mass m^* and the deformation-potential constant E_1 have an essential influence on the mobility. Their dependences on the bandgap in AGNRs can be well understood within the framework of a tight-binding (TB) model.

According to the analysis[24] of a TB model that considers the hopping between the nearest-neighbor π electrons, the electronic structure of graphene and AGNRs can be briefly summarized as follows (see also Fig. 1). The energy dispersion of graphene near the Fermi points is expressed as Dirac cones:

$$E(\mathbf{k}) = E_0 \pm \frac{3}{2} t_0 r_0 |\mathbf{k} - \mathbf{k}_F|, \tag{2}$$

where E_0 is the on-site energy which is equal to the Fermi energy E_F, t_0 is the hopping parameter, and r_0 is the equilibrium bond length. In this study, we adopted $t_0 = 2.67$ eV from Li *et al.*,[24] which was obtained by fitting Eq. (2) with DFT calculation results. For AGNRs, the $\mathbf{k}$ value of the allowed electronic states lies on some discrete straight lines due to quantum confinement, so their band structure is composed of some cut sections of the graphene's Dirac cones. When a strain is exerted, the Dirac cones shift in the ($\mathbf{k}$, E) space. Graphene, thus, remains gapless under strain. For AGNRs, because the allowed k-lines are fixed in the space, the shift in the Dirac cones under strain will make the bandgap of AGNRs smaller or larger. Based on these facts, we can deduce expressions for m^* and E_1.

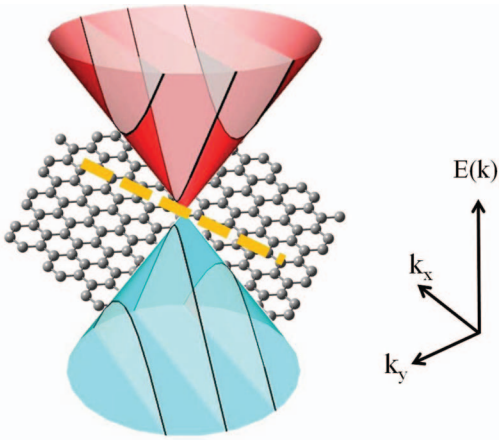

FIG. 1. Schematic illustration of the electronic structure of graphene and AGNRs. The electronic structure of graphene is represented by 2D cones, and that for AGNRs by a set of discrete lines on the cones cut by allowed k-lines. Under a strain, the cones would shift in the $E(k)$-k space, where the trajectory of the Dirac point is illustrated by the thick dashed yellow line.

Because only some discrete k-lines are allowed for AGNRs, their conduction and valence bands can be written from Eq. (2) as

$$E(k_x) = E_0 \pm \frac{1}{2}\sqrt{9t_0^2 r_0^2 k_x^2 + E_g^2}, \tag{3}$$

where E_g is the bandgap and the ribbon axis is aligned along the x-direction. The effective mass is easily derived:

$$m^* = \frac{2\hbar^2}{9t_0^2 r_0^2} E_g, \tag{4}$$

giving a linear relation between m^* and E_g. Equation (4) is also valid for single-layer h-BN under TB approximation.

The band-edge energy of AGNRs is from Eq. (3) determined by both the Fermi energy ($E_F \equiv E_0$) and the bandgap as

$$E_{\text{edge}} = E_F \pm \frac{1}{2} E_g, \tag{5}$$

where "+" applies for electron carriers (the conduction band), whereas "–" applies for hole carriers (the valence band). Therefore, the deformation-potential constant E_1 is derived as

$$E_1 = \frac{\partial E_{\text{edge}}}{\partial \varepsilon} = \frac{\partial E_F}{\partial \varepsilon} \pm \frac{1}{2}\frac{\partial E_g}{\partial \varepsilon}. \tag{6}$$

According to the TB analysis in Ref. 24, the dependence of the gap on the strain is given as

$$\frac{\partial E_g}{\partial \varepsilon} = \pm 3 t_0 S_t (1 + \nu_A), \tag{7}$$

where $S_t \approx 1.29$ is a constant reflecting the dependence of the hopping parameter on the bond length and $\nu_A \approx 0.145$ is the Poisson's ratio. The assignment of "±" in Eq. (7) depends on the relative position between the allowed k-lines and the Dirac points and varies periodically with ribbon width N_A, i.e., "+" for $N_A = 3p$ and "−" for $N_A = 3p + 1$, $3p + 2$, where p is an integer.[24] Equation (6) indicates that E_1 for electrons and holes are different for AGNRs. This greatly affects the polarity of the transport as will be shown below.

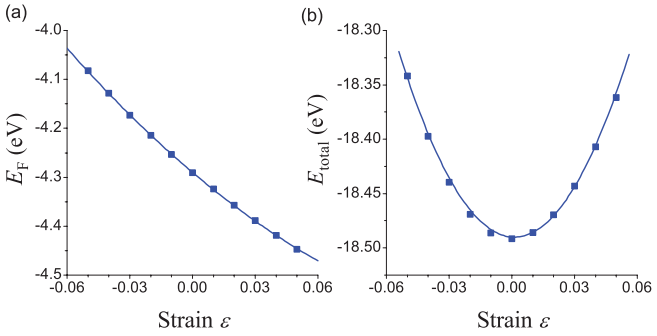

FIG. 2. The calculated Fermi energy (E_F) and total energy (E_{total}) of graphene as a function of the uniaxial strain ε. The solid blue lines are quadratic fittings to the data.

By substituting Eqs. (4), (6), and (7) into Eq. (1), we obtain the TB prediction for AGNR mobility:

$$\mu = \frac{27et_0^3r_0^3C}{(16\pi k_BT)^{\frac{1}{2}}\hbar\left(\frac{\partial E_F}{\partial\varepsilon} \pm \frac{3}{2}t_0S_t(1+\nu_A)\right)^2 E_g^{3/2}}. \quad (8)$$

III. RESULTS AND DISCUSSION

A. Graphene: Extraction of parameters for TB analysis

Many electronic properties of AGNRs originate from graphene. Therefore, we first conducted DFT calculations on related properties of infinite graphene sheet (Fig. 2). The Fermi energy E_F decreases almost linearly with increasing uniaxial strain ε (Fig. 2(a)). The deviation from a linear law is slight under small ε as seen from a quadratic fitting result, $E_F = 10.1\varepsilon^2 - 3.62\varepsilon - 4.29$ eV. By ignoring the nonlinearity, we obtained $\partial E_F/\partial\varepsilon = -3.62$ eV, which would be used in the TB analysis. In contrast, the total energy E_{total} (Fig. 2(b)) obeys a typical quadratic law. The corresponding stretching modulus of graphene ($C_{graphene}$) was found to be 112 eV/S (where $S = 5.27 \times 10^{-20}$ m^2 is the area of a unit cell with two carbon atoms), or equivalently, 339 J/m^2, which is consistent with the experimental measurement.[31] This value is useful in estimating the stretching modulus C for GNRs.

B. AGNRs: The mobility and its determinants

We now examine the transport properties of AGNRs. We conducted DFT calculations on AGNRs with various ribbon widths to calculate the mobility and the related quantities. We found that the DFT results are well described by the TB theory (Fig. 3).

The TB approach predicts that m^* is proportional to E_g (Eq. (4)). The DFT calculations indeed confirmed such a trend (Fig. 3(a)). By adopting $t_0 = 2.67$ eV from the literature,[24] the quantitative agreement between TB prediction and DFT calculations is reasonable considering that t_0 is optimized for graphene but not for AGNRs. For $\mathbf{k}$ far away from $\mathbf{k}_F$, the band structure of graphene would deviate from the Dirac cones,[32] which will contribute to the discrepancy between Eq. (4) and the DFT results for large E_g.

The calculated deformation-potential constant E_1 of AGNRs displays a periodic oscillating behavior as N_A increases (Fig. 3(b)), which is consistent with the observation of Long *et al.*[20] From Eq. (7), we obtained the TB prediction of $\partial E_g/\partial\varepsilon = \pm 11.8$ eV. Together with the parameter of $\partial E_F/\partial\varepsilon = -3.62$ eV obtained above, the TB prediction using Eq. (6) gives that $E_1 = -3.62 \pm 11.8/2 = 2.30, -9.54$ eV. This prediction agrees well with the DFT results (Fig. 3(b)). Also, the oscillation in E_1 as a function of N_A is understood to come from the sign of $\partial E_g/\partial\varepsilon$, which is determined by the position of the allowed k-lines for AGNRs.[24]

To calculate the mobility of AGNRs from Eq. (1), one also needs the stretching modulus C. C can be obtained directly from DFT calculation of AGNRs or can be estimated from the properties of graphene:

$$C = C_{graphene}d = \frac{\sqrt{3}}{2}N_Ar_0C_{graphene}, \quad (9)$$

where d is the width of the AGNR and $C_{graphene} = 339$ J/m^2 is the stretching modulus of graphene determined above. A numerical comparison verified that two approaches are consistent (see Fig. S1 in supplementary material[33]). To make the analysis more concise, we adopted $C = 8.36 \times 10^{-7}$ J/m from Eq. (9) with $N_A = 20$. The mobility prediction (Eq. (8)) can then be evaluated with all known parameters

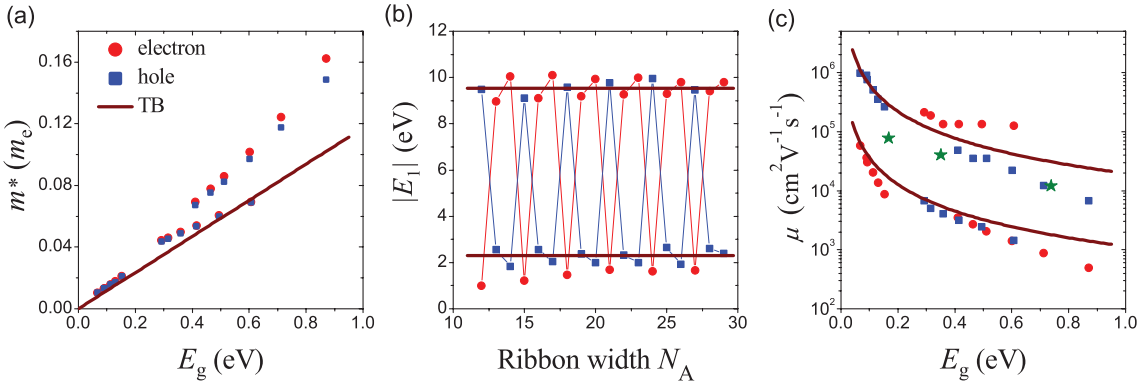

FIG. 3. Electronic properties of AGNRs with ribbon width $N_A = 12$–29: (a) the effective mass m^* (in units of m_e, the mass of the free electron); (b) the deformation-potential constant E_1; and (c) the carrier mobility μ. Data from DFT calculations are plotted as symbols (red circles for properties of electrons and blue squares for holes), whereas the TB predictions (Eqs. (4) and (6)–(8)) are plotted in thick brown lines. In the panel (c), data of bulk III-V semiconductors (InSb, InAs, $In_{0.53}Ga_{0.47}As$)[15] were also included for comparison as green stars.

to be

$$\mu = 0.114 \times 10^4 \times E_g^{-3/2}, \quad 1.96 \times 10^4 \times E_g^{-3/2}, \qquad (10)$$

where the units used for μ and E_g are $cm^2\ V^{-1}\ s^{-1}$ and eV, respectively. A comparison between the TB prediction and the DFT numerical data is provided in Fig. 3(c). Clearly, the TB model captures the main characteristics of μ: there are two branches for μ, and μ decreases with increasing E_g in each branch. From the TB analysis, the former characteristic comes from E_1 (which further originates from the existence of the term $\partial E_g/\partial\varepsilon$ in Eq. (6)), whereas the latter originates from the linear relationship between m^* and E_g. In Fig. 3(c), we also included the data of a few bulk III-V semiconductors for comparison. This demonstrates that the high branch of μ for AGNRs is higher than or comparable to that of III-V semiconductors under the same E_g.

C. Strain effect: The switch of transport polarity in AGNRs

Long *et al.*[20] demonstrated that the transport polarity (i.e., whether electron or hole transport is determined by the mobility difference between electrons and holes) of AGNRs oscillates as a function of N_A. From the TB analysis above, one can understand that the origin of the polarity is the dependence of E_g on ε (Eq. (6)). Thus, the expectation is that any means to change the sign of $\partial E_g/\partial\varepsilon$ would switch the transport polarity.

Strain has important effects on the electronic and transport properties of graphene and GNRs.[24,34,35] Under the exertion of a uniaxial strain, E_g of AGNRs was effectively modified in a periodic zigzag pattern.[24] Accordingly, the sign of $\partial E_g/\partial\varepsilon$ would change at each turning point. Therefore, strain may act as an effective method in modifying the transport polarity of AGNRs.

We have investigated the strain effect on the mobility of AGNRs. As an example, the results of the system with $N_A = 18$ were given in Fig. 4. The mobility of electrons and holes spans about three orders of magnitudes under the strain and resides on two branches. More importantly, the transport polarity switches at around $\varepsilon \approx 0.033$, where E_g reaches its maximum: the electron mobility jumps from the high branch to the low branch, whereas holes experience a reverse process. Similar switches also occur at the other two ε values where E_g reaches its minimum.

It has been proposed that strain can be used to generate various basic elements for all-graphene electronics.[34] Strain in tuning the transport polarity provides a useful means for strain engineering of graphene.

D. Possible extensions

The properties revealed above for 1D AGNRs are applicable for other systems. Here, we present a brief analysis for two examples.

One example is the 2D functionalized graphene systems. We calculated the electronic structure of BN-embedded graphene (BNG),[11] Janus-type mosaic graphene (J-MOG)

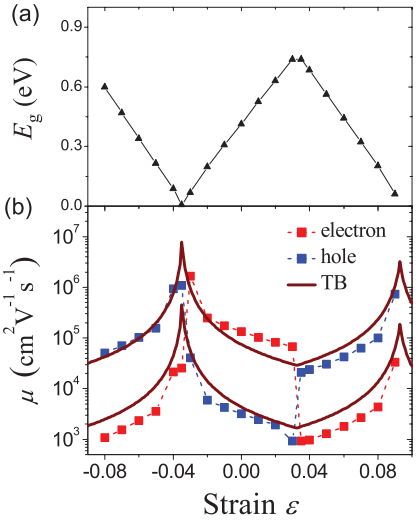

FIG. 4. (a) The bandgap and (b) the carrier mobility of AGNRs with $N_A = 18$ as a function of the uniaxial strain.

with hydrogenation and/or fluorination,[36] and graphene antidot lattices (GALs).[37] The results are displayed in Fig. 5(a). A linear relation between m^* and E_g is clearly seen, which would contribute to the inverse relationship between mobility and bandgap. The other example is three-dimensional (3D) III-V semiconductor compounds. We extracted experimental data from Schwierz[15] and redrawn them in Fig. 5(b). μ decreases with increasing E_g, and the data are well described by a reverse law of $\mu \propto E_g^{-3/2}$ (solid line in Fig. 5(b)) as AGNRs. Note that the deformation potential theory[25] predicts the form $\mu \propto E_g^{-5/2}$ in 3D compounds, so it is unclear why III-V semiconductor compounds obey a law similar to the 1D AGNRs. This deserves further investigations.

E. How can we realize high mobility in graphene systems?

The ultrahigh mobility of graphene can be attributed to two reasons: (1) the high C value since graphene is the

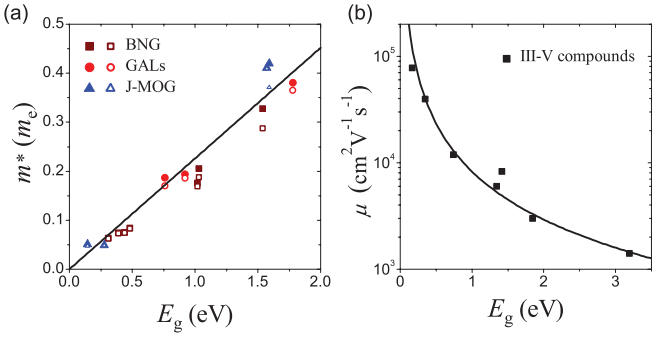

FIG. 5. (a) The correlation between m^* and E_g for various two-dimensional functionalized graphene systems: BN-embedded graphene (BNG), graphene antidot lattices (GALs), and Janus-type mosaic graphene (J-MOG) (detailed data is provided in supplementary material[33]). Calculated data for electrons and holes are plotted in filled and opened symbols, respectively. The solid line is a linear fit to the data. (b) The correlation between μ and E_g for bulk III-V compounds: (from left to right) InSb, InAs, $In_{0.53}Ga_{0.47}As$, InP, GaAs, $In_{0.49}Ga_{0.51}P$, and GaN. Data came from Schwierz,[15] and the solid line is the fitted result $\mu = 0.83 \times 10^4 \times E_g^{-3/2}$.

strongest material ever measured;[31] (2) the zero m^*. However, opening bandgap in graphene systems enables carriers to gain nonzero m^* and then leads to the degradation of mobility. Based on Eq. (4), we rated the contribution of m^* to μ in AGNRs as not superior to that in other systems under the same E_g because the differences in t_0 for various systems are usually not large, e.g., $t_0 \approx 2.40$ eV for h-BN. But the E_1 can vary in a wide range and leads to two μ branches with difference more than 1 order of magnitude in AGNRs. As above, E_1 is expressed as the difference (for hole) or sum (for electron) between two terms: $\partial E_F/\partial\varepsilon$, $\partial E_g/2\partial\varepsilon$ (Eq. (6)). The first term, $\partial E_F/\partial\varepsilon$, is an inner characteristic of graphene, but the second term can be affected by ribbon width, edge passivation, and edge structure.[38,39] According to our calculations, the transport polarity is determined by the sign of $\partial E_g/\partial\varepsilon$. Moreover, if the absolute value of $\partial E_g/\partial\varepsilon$ is closer to 7 eV, a lower E_1 either for electron or for hole will be attained and the corresponding mobility will be higher. The expression of E_1 can be extended to other two-dimensional graphene systems. For example, a stretched boron-nitride-embedded graphene whose $\partial E_g/\partial\varepsilon$ is 6 eV has hole mobility comparable to that of graphene when the bandgap is 1.0 eV.[40] Thus, an effective regulation of E_1 is essential for achieving both high mobility and large on-off ratio in graphene devices.

IV. CONCLUSION

We have investigated the mobility properties of AGNRs by combining DFT calculations and a TB model analysis. We demonstrated that the inverse relationship between μ and E_g is caused by an intrinsic linear dependence of m^* on E_g, and that E_1 is responsible for the existence of two μ branches. We also showed that strain is effective in switching the transport polarity of AGNRs.

ACKNOWLEDGMENTS

We thank Professor Zhigang Shuai and Dr. Jinyang Xi for their assistance in the DFT calculations of mobility. This work was supported by the National Natural Science Foundation of China (Grant Nos. 51121091 and 20973013) and the Ministry of Science and Technology of China (Grant Nos. 2013CB932603 and 2012CB933404).

[1] K. I. Bolotin, K. J. Sikes, Z. Jiang, M. Klima, G. Fudenberg, J. Hone, P. Kim, and H. L. Stormer, Solid State Commun. **146**, 351 (2008).
[2] S. V. Morozov, K. S. Novoselov, M. I. Katsnelson, F. Schedin, D. C. Elias, J. A. Jaszczak, and A. K. Geim, Phys. Rev. Lett. **100**, 016602 (2008).
[3] J.-H. Chen, C. Jang, S. D. Xiao, M. Ishigami, and M. S. Fuhrer, Nat. Nanotechnol. **3**, 206 (2008).
[4] C. R. Dean, A. F. Young, I. Meric, C. Lee, L. Wang, S. Sorgenfrei, K. Watanabe, T. Taniguchi, P. Kim, K. L. Shepard, and J. Hone, Nat. Nanotechnol. **5**, 722 (2010).
[5] M. Y. Han, B. Özyilmaz, Y. B. Zhang, and P. Kim, Phys. Rev. Lett. **98**, 206805 (2007).
[6] Q. M. Yan, B. Huang, J. Yu, F. W. Zheng, J. Zang, J. Wu, B. L. Gu, F. Liu, and W. H. Duan, Nano. Lett. **7**, 1469 (2007).
[7] D. C. Elias, R. R. Nair, T. M. G. Mohiuddin, S. V. Morozov, P. Blake, M. P. Halsall, A. C. Ferrari, D. W. Boukhvalov, M. I. Katsnelson, A. K. Geim, and K. S. Novoselov, Science **323**, 610 (2009).
[8] E. Bekyarova, M. E. Itkis, P. Ramesh, C. Berger, M. Sprinkle, W. A. de Heer, and R. C. Haddon, J. Am. Chem. Soc. **131**, 1336 (2009).
[9] M. M. Yang, L. Zhou, J. Y. Wang, Z. F. Liu, and Z. R. Liu, J. Phys. Chem. C **116**, 844 (2012).
[10] L. Ci, L. Song, C. H. Jin, D. Jariwala, D. X. Wu, Y. J. Li, A. Srivastava, Z. F. Wang, K. Storr, L. Balicas, F. Liu, and P. M. Ajayan, Nat. Mater. **9**, 430 (2010).
[11] R. Q. Zhao, J. Y. Wang, M. M. Yang, Z. F. Liu, and Z. R. Liu, J. Phys. Chem. C **116**, 7581 (2012).
[12] X. R. Wang, Y. J. Ouyang, X. L. Li, H. L. Wang, J. Guo, and H. J. Dai, Phys. Rev. Lett. **100**, 206803 (2008).
[13] B. Obradovic, R. Kotlyar, F. Heinz, P. Matagne, T. Rakshit, M. D. Giles, M. A. Stettler, and D. E. Nikonov, Appl. Phys. Lett. **88**, 142102 (2006).
[14] A. Betti, G. Fiori, and G. Iannaccone, Appl. Phys. Lett. **98**, 212111 (2011).
[15] F. Schwierz, Nat. Nanotechnol. **5**, 487 (2010).
[16] J.-H. Chen, C. Jang, S. Adam, M. S. Fuhrer, E. D. Williams, and M. Ishigami, Nat. Phys. **4**, 377 (2008).
[17] S. Adam, E. H. Hwang, V. M. Galitski, and S. Das Sarma, Proc. Natl. Acad. Sci. U.S.A. **104**, 18392 (2007).
[18] Z. Jin, J. Yao, C. Kittrell, and J. M. Tour, ACS Nano **5**, 4112 (2011).
[19] S. Das Sarma, S. Adam, E. H. Hwang, and E. Rossi, Rev. Mod. Phys. **83**, 407 (2011).
[20] M. Q. Long, L. Tang, D. Wang, L. J. Wang, and Z. G. Shuai, J. Am. Chem. Soc. **131**, 17728 (2009).
[21] K. M. Borysenko, J. T. Mullen, E. A. Barry, S. Paul, Y. G. Semenov, J. M. Zavada, M. B. Nardelli, and K. W. Kim, Phys. Rev. B **81**, 121412 (2010).
[22] E. V. Castro, H. Ochoa, M. I. Katsnelson, R. V. Gorbachev, D. C. Elias, K. S. Novoselov, A. K. Geim, and F. Guinea, Phys. Rev. Lett. **105**, 266601 (2010).
[23] A. H. C. Neto, F. Guinea, N. M. R. Peres, K. S. Novoselov, and A. K. Geim, Rev. Mod. Phys. **81**, 109 (2009).
[24] Y. Li, X. W. Jiang, Z. F. Liu, and Z. R. Liu, Nano Res. **3**, 545 (2010).
[25] J. Bardeen and W. Shockley, Phys. Rev. **80**, 72 (1950).
[26] F. B. Beleznay, F. Bogár, and J. Ladik, J. Chem. Phys. **119**, 5690 (2003).
[27] M. Q. Long, L. Tang, D. Wang, Y. L. Li, and Z. G. Shuai, ACS Nano **5**, 2593 (2011).
[28] G. Kresse and J. Furthmüller, Comput. Mater. Sci. **6**, 15 (1996).
[29] G. Kresse and D. Joubert, Phys. Rev. B **59**, 1758 (1999).
[30] J. P. Perdew and Y. Wang, Phys. Rev. B **45**, 13244 (1992).
[31] C. Lee, X. D. Wei, J. W. Kysar, and J. Hone, Science **321**, 385 (2008).
[32] After considering the deviation from the Dirac cones, the TB model gives $m^* = \frac{4\hbar^2 E_g}{9(2t_0^2 \pm t_0 E_g) r_0^2}$.
[33] See supplemental material at http://dx.doi.org/10.1063/1.4792142 for a numerical comparison of the TB prediction and DFT results for the stretching modulus of AGNRs, schematic views of various 2D functionalized graphene systems, and a table of their bandgap.
[34] V. M. Pereira and A. H. Castro Neto, Phys. Rev. Lett. **103**, 046801 (2009).
[35] J. Y. Wang, Z. F. Liu, and Z. R. Liu, AIP Adv. **2**, 012103 (2012).
[36] M. M. Yang, R. Q. Zhao, J. Y. Wang, L. M. Zhang, Q. Xie, Z. F. Liu, and Z. R. Liu, "Bandgap opening by Janus-faced mosaic graphene," J. Appl. Phys. (in press).
[37] F. P. Ouyang, S. L. Peng, Z. F. Liu, and Z. R. Liu, ACS Nano **5**, 4023 (2011).
[38] X. H. Peng and S. Velasquez, Appl. Phys. Lett. **98**, 023112 (2011).
[39] Y. C. Cheng, H. T. Wang, Z. Y. Zhu, Y. H. Zhu, Y. Han, X. X. Zhang, and U. Schwingenschlogl, Phys. Rev. B **85**, 073406 (2012).
[40] J. Y. Wang, R. Q. Zhao, Z. F. Liu, and Z. R. Liu, "Widely tunable carrier mobility of boron-nitride-embedded graphene," Small (in press).